B- and T-cell acute lymphoblastic leukemias evade chemotherapy at distinct sites in the bone marrow

Malwine J. Barz,[1*] Lena Behrmann,[1*] Danaëlle Capron,[1*] Gabriele Zuchtriegel,[1*] Fabio D. Steffen,[1] Leo Kunz,[2] Yang Zhang,[2] Iria Jimenez Vermeerbergen,[1] Blerim Marovca,[1] Moritz Kirschmann,[3] Antonia Zech,[1] César Nombela-Arrieta,[4] Urs Ziegler,[3] Timm Schroeder,[2] Beat Bornhauser[1] and Jean-Pierre Bourquin[1]

[1]University Children's Hospital Zürich, Pediatric Oncology and Children's Research Center, Balgrist Campus AG, Zürich; [2]ETH Zürich, Department of Biosystems Science and Engineering, Basel; [3]University of Zürich, Center for Microscopy and Image Analysis, Zürich and [4]University Hospital Zürich, Division of Hematology, Zürich, Switzerland

**MJB, LB, DC and GZ contributed equally and are listed in alphabetical order.*

Correspondence: J-P. Bourquin
jean-pierre.bourquin@kispi.uzh.ch

Received: December 2, 2021.
Accepted: October 14, 2022.
Early view: November 3, 2022.

https://doi.org/10.3324/haematol.2021.280451

Supplemental Material

B and T cell acute lymphoblastic leukemia survive chemotherapy at different sites in the bone marrow

Barz et al.

B and T cell acute lymphoblastic leukemia evade chemotherapy at distinct sites in the bone marrow

Malwine J. Barz[1]*, Lena Behrmann[1]*, Danaëlle Capron[1]*, Gabriele Zuchtriegel[1]*, Fabio D. Steffen[1], Leo Kunz[2], Yang Zhang[2], Iria Jimenez Vermeerbergen[1], Blerim Marovca[1], Moritz Kirschmann[3], Antonia Zech[1], César Nombela-Arrieta[4], Urs Ziegler[3], Timm Schroeder[2], Beat Bornhauser[1] and Jean-Pierre Bourquin[1#]

[1]University Children's Hospital Zürich, Pediatric Oncology and Children's Research Center, Balgrist Campus AG, Lengghalde 5, 8008 Zürich, Switzerland

[2]ETH Zürich, Department of Biosystems Science and Engineering, Basel, Switzerland

[3]University of Zürich, Center for Microscopy and Image Analysis, Zürich, Switzerland

[4]University Hospital Zürich, Division of Hematology, Zürich, Switzerland

* M.J.B, L.B., D.C. and G.Z contributed equally and are listed in alphabetical order

[#]corresponding author

Corresponding Author

Jean-Pierre Bourquin, jean-pierre.bourquin@kispi.uzh.ch

University Children's Hospital Zürich

Steinwiesstrasse 75

CH-8032 Zürich, Switzerland

Phone, +41 44 266 7304

Fax, +41 44 266 7171

Supplementary Material and Methods

Mice and xenotransplantation

The original *NESTIN*-GFP strain is from Dr. G. Enikolopov and was back-crossed to NOD.Cg-*Prkdc*$_{scid}$ *IL2rg*$_{tm1Wjl}$/SzJ (NSG) background at the BRF, The Francis Crick Institute (unpublished data). All animals were kept and bred at the University Children's Hospital Zürich animal facility according to institutional animal care guidelines. Transplanted animals were kept under antibiotic prophylaxis (Baytril, 0.005%). For xenotransplantation Patient derived xenograft (PDX) cells were recovered from cryopreserved early passage PDX samples. Cell viability was assessed using trypan blue staining after thawing. One million live cells of indicated patient-derived BCP- and T-ALL cells were transplanted intravenously in 100 µl PBS in the tail vein of NSG mice. For studying early engraftment of leukemic cells mice were sacrificed at day 11 (BCP-ALL) or day 4 (T-ALL) and femurs were harvested for 3D confocal microscopy and tibiae were flushed for flow cytometry. For studying MRD, mice were engrafted for 11 days and treated for indicated times with dexamethasone (Mephameson; mepha, 4 mg/ml) at 10.5 mg/kg intraperitoneal (IP), doxorubicin (Doxorubicin; Sandoz, 2 mg/ml) at 2 mg/kg intravenous (IV) and vincristine (Vincristine-Teva; Teva Pharma, 1 mg/kg) at 0.5 mg/kg IP. Health status was examined weakly by body weight measurement. For re-transplantation of chemotherapy selected cells, bone marrow of one femur and one tibia were harvested after treatment and re-transplanted unpurified bone marrow in a new recipient mouse. Leukemia burden was monitored weekly in the peripheral blood.

Generation of Luc2-eGFP PDX

Viral particles were produced using 293T cells after transfection with ProFection Mammalian Transfection System – Calcium Phosphate (Promega) as published before [1]. pSLIG (SFFV-Luc2-IRES-eGFP), pMD2.G and psPAX2 plasmids were used for lentivirus production. Viral supernatants were harvested 24 h after transfection. For transduction, ALL cells were cultured in viral supernatant for 24 h with subsequent transplantation. After expansion in NSG mice, cells were harvested, purified by flow cytometry sort and re-transplanted for expansion of a pure population.

Bioluminescence *in vivo* imaging

Mice were anesthetized using 2.5% isoflurane and injected intravenously with D-luciferin (100 µl RediJect D-luciferin Bioluminescent substrate; Perkin Elmer). Exactly one minute after intravenous substrate injection, mice were imaged using the IVIS Lumina II Imaging System (Caliper Life Sciences). Images were acquired in a heated, light-tight chamber. The Living

Image software 4.5 (Caliper Life Sciences) was used for data acquisition and quantification of light emission. Different regions of interest (ROI) were defined and signals were considered positive, when light emission exceeded background in each ROI; background was measured in 15 mice harboring luciferase negative leukemias.

In vivo tracing of leukemic cells

Patient-derived BCP- and T-ALL cells were stained with CellTrace™ Violet Cell Proliferation Kit (ThermoFisher, C34557, 5 µM) for 20 minutes at room temperature and washed with PBS according to the manufacturer's instructions. Successful labeling of leukemic cells with CFSE was validated by flow cytometry prior to intravenous transplantation of $1x10^7$ (for short-term treatment) or $1x10^6$ cells (for induction chemotherapy) into NSG mice. For short-term treatment mice were engrafted for 7 days and then treated with dexamethasone (Mephameson; mepha, 4 mg/ml; day 1, 2, 3), vincristine (Teva Pharma, 1 mg/kg; day 1), and doxorubicin (Sandoz 2 mg/ml; day 1). For full induction chemotherapy, mice were engrafted for 11 days and then received standard chemotherapy according to the treatment protocol for studying MRD, as described above. After short-term (3 days) or induction chemotherapy mice were euthanized by CO_2 asphyxiation and femurs were harvested. One femur was kept for 3D confocal microscopy, the other femur was crushed and analyzed by flow cytometry. Proportions of CFSE-positive cells were determined by analyzing numbers of CFSE positive cells normalized to hCD45-positive cells. To set the gate for CFSE-positive cells, CFSE intensity was measured prior to intravenous transplantation. The gate of CFSE-positive cells was set to include all cells harboring high CFSE signal [2,3]. All further analyses were done and analyzed with the same instrument settings and gates.

Flow Cytometry

Human engraftment was determined in bone marrow harvested from tibiae. Single cells were isolated by flushing the bone marrow with PBS or crushing the bones using a mortar. Spleen cell suspensions were prepared by tamping the tissue through a nylon mesh. Mononucleated cells from blood were obtained by red blood cell lysis. Human engraftment was monitored as the percentage of human cells over all human (anti-human-CD19 PE, BioLegend; anti-human-CD7 PE, ebiosciences; anti-human-CD45 Alexa Fluor 647, BioLegend) and murine leukocytes (anti-mouse-CD45 eFluor 450, ebiosciences). Flow Cytometry was performed on a BD FACS Canto II and BD LSRFortessa (BD Biosciences) and analyzed with FlowJo.

Drug response profiling

In vivo chemotherapy selected PDX cells were recovered from spleens of mice and cryopreserved. Cells were thawed and viability was assessed with trypan blue. Drug response was assessed as described previously.[4] In brief, $2.5x10^3$ hTERT-MSC were plated in 30 µl serum free AIMV medium (ThermoFisher) in a 384-well plate. The following day, $2.5x10^4$ primary cells in 32.5 µl AIMV-medium were added. After 24 h incubation, cocultured cells were treated for 72 h with indicated drugs. Viability was assessed using CyQUANT (ThermoFisher) and quantified using high content fluorescence microscopy (ImageXpress, Molecular Devices). Drug response profiles are determined by fitting a three-parameter dose response model (log IC50, I_{max} and n) to DMSO normalized cell counts.

Bone preparation for imaging

Bones were isolated and fixed immediately for 24 h in 1% paraformaldehyde-lysine-periodate (PLP) fixative. After fixation, bones were cryoprotected in a 20% sucrose solution for 48 h and snap frozen in OCT (TissueTek). Frozen bones were cut from both sides using a Cryostat (Leica CM1850) to obtain thick bone marrow sections. OCT was washed off in PBS, blocking in 10% donkey serum/0.2% Triton X/PBS for 24 h. Bone sections were then incubated with primary antibodies diluted in blocking buffer with or without DAPI (4',6-diamidino-2-phenylindole) for 24 h and washed 3 x 1 h with PBS. After washing steps, bone sections were incubated with secondary antibodies for 24 h, washed 3 x 1 h in PBS at 4°C and subsequently cleared in RapiClear 1.52 (CamBioSciences) overnight. Thick sections were then embedded in RapiClear 1.52 for subsequent imaging. The following primary antibodies were used for IF: anti-human-CD45 (clone MEM-28; abcam; 1:200), anti-mouse-endoglin (polyclonal, AF1320, R&D; 1:200), anti-mouse-perilipin (D1D8, Cell Signalling; 1:200), anti-mouse-laminin (L9393, Sigma Aldrich; 1:150), anti-mouse-collagen type I (CL50151AP, Cedarlanlabs; 1:200), anti-mouse-endomucin (clone V.7C7; sc-65495, Santa Cruz biotechnology; 1:75), anti-mouse-osterix (polyclonal, NBP2-38019, Novus biologicals; 1:200). The following secondaries antibodies were used for IF: donkey-anti-mouse Alexa Fluor 488, donkey-anti-mouse Alexa Fluor 568, donkey-anti-goat Alexa Fluor 647, donkey-anti-rabbit Alexa Fluor 488, donkey-anti-rabbit Alexa Fluor 568, donkey-anti-rat Alexa Fluor 488 (all Invitrogen; 1:400).

Confocal imaging of thick section

3D confocal microscopy of the bone marrow was performed using Leica SP8 inverse resonant scanning confocal microscope. All images were acquired with the following specifications: HyD and PMT detectors, laser lines 405 nm, 488 nm, 552 nm and 638 nm. For each bone, distal epiphysis, distal metaphysis and part of the diaphysis were imaged using tiled z-stack imaging.

All z-stacks were between 100 - 300 µm of thickness. Images were acquired with an HC PL APO C52 L20x/0.75 immersion objective, 1024x1024 pixels resolution with 1.5-2.0 µm z-step, 1.25 zoom factor, pinhole size: 1 Airy Unit, using 8x line averaging and bidirectional scanning.

Image annotation

All tiled z-stack images were modeled in 3D using Imaris (Version 9.1.0, Oxford Instruments). Sinusoids were defined as endoglin positive or endoglin^{high}endomucin^{low}, transition zones as endoglin^{low}endomucin^{high}, nestin-associated vessels were defined as nestin-GFP^{+}endomucin^{-} endoglin regions. Endosteal space was defined as collagen type I positive structures or delimited using DAPI and osterix co-staining. Leukemic cells were defined as hCD45^{+} cells with a round morphology. Slow proliferating cells were identified by co-expression of hCD45 on the cell surface and CFSE throughout the cells.

References

1. Behrmann L, McComb S, Aguadé-Gorgorió J, et al. Efficient Generation of Multi-gene Knockout Cell Lines and Patient-derived Xenografts Using Multi-colored Lenti-CRISPR-Cas9. Bio-Protoc 2017;7(7):e2222.

2. Duan C-W, Shi J, Chen J, et al. Leukemia Propagating Cells Rebuild an Evolving Niche in Response to Therapy. Cancer Cell 2014;25(6):778–793.

3. Kunz L, Schroeder T. A 3D Tissue-wide Digital Imaging Pipeline for Quantitation of Secreted Molecules Shows Absence of CXCL12 Gradients in Bone Marrow. Cell Stem Cell 2019;25(6):846-854.e4.

4. Frismantas V, Dobay MP, Rinaldi A, et al. Ex vivo drug response profiling detects recurrent sensitivity patterns in drug-resistant acute lymphoblastic leukemia. Blood 2017;129(11):e26–e37.

5. Coutu DL, Kokkaliaris KD, Kunz L, Schroeder T. Multicolor quantitative confocal imaging cytometry. Nat Methods 2018;15(1):39–46.

6. Fischer U, Forster M, Rinaldi A, et al. Genomics and drug profiling of fatal TCF3-HLF−positive acute lymphoblastic leukemia identifies recurrent mutation patterns and therapeutic options. Nat Genet 2015;47(9):1020–1029.

Supplementary Tables

Table S1. Patient characteristics

Patient ID	origin	Immuno-phenotype	Cytogenetic subtype	Prednisolone response	outcome	ALL-BFM 2000 risk group	Genetic data
B-VHR-12	d	BCP-ALL	other*	good	Relapse	VHR	not available
B-VHR-10	d	BCP-ALL	other*	poor	CCR	VHR	not available
B-SR-22	d	BCP-ALL	*E2A-PBX1*	poor	CCR after SCT	SR	Fischer et al.[6]
B-HR-31	d	BCP-ALL	*KMT2A-AF4*	good	SCT	HR	not available
B-VHR-20	d	BCP-ALL	*E2A-HLF*	good	TRM	VHR	Fischer et al.[6]
B-VHR-21	d	BCP-ALL	*E2A-HLF*	good	TRM	VHR	Fischer et al.[6]
B-VHR-24	d	BCP-ALL	*E2A-HLF*	good	Relapse	VHR	Fischer et al.[6]
B-SR-21	d	BCP-ALL	*E2A-PBX1*	good	CCR	SR	Fischer et al.[6]
B-R-03	r	BCP-ALL	high hyperdiploid	na	Nonresponse	na	not available
T-HR-04	d	pre T-ALL	*SIL-TAL*	poor	CCR	HR	not available
T-VHR-04	d	cortical T-ALL	*SIL-TAL*	na	na	VHR	not available
T-VHR-09	d	cortical T-ALL	other*	poor	CCR	VHR	not available
T-VHR-01	r	cortical T-ALL	*SIL-TAL*	na	na	na	not available
T-MR-09	d	cortical T-ALL	*LMO2-RAG2**	poor	Relapse	MR	not available

*Original samples were obtained at diagnosis (d) or at relapse (r). Risk stratification according to ALL-BFM 2000 is indicated as follows: very high risk (VHR), high risk (HR), medium risk (MR) and standard risk (SR). *represents ALL lacking the established cytogenetic abnormalities (for BCP-ALL: E2A-PBX1, E2A-HLF, BCR-ABL1, KMT2A-rearrangement, ETV6-RUNX1, high hyperdiploid or hypodiploid; T-ALL: SIL-TAL). Abbreviations: CCR, continued complete remission; SCT, stem cell transplantation; TRM, treatment-related mortality; nd, not determined; na, not available.*

Table S2. Central nervous system (CNS) infiltration of xenografted mice

Patient ID	Origin	Immuno-phenotype	Cytogenetic subtype	Transplatation	ALL-BFM 2000 risk group	Brain HE
B-SR-01	d	BCP-ALL	other*	primary	SR	leukemia positive
B-SR-13	d	BCP-ALL	other*	secondary	SR	leukemia positive
B-MR-19	d	BCP-ALL	other*	primary	MR	leukemia positive
B-MR-19	d	BCP-ALL	other*	tertiary	MR	leukemia positive
B-MR-19	d	BCP-ALL	other*	tertiary	MR	leukemia positive
B-HR-15	d	BCP-ALL	other*	primary	MR	leukemia negative
B-HR-17	d	BCP-ALL	other*	primary	MR	leukemia positive
B-HR-17	d	BCP-ALL	other*	primary	MR	leukemia positive
B-HR-17	d	BCP-ALL	other*	secondary	MR	leukemia positive
B-HR-14	d	BCP-ALL	other*	primary	HR	leukemia positive
B-HR16	d	BCP-ALL	other*	primary	HR	leukemia positive
B-VHR-28	d	BCP-ALL	other*	secondary	VHR	leukemia positive
B-R-22	r	BCP-ALL	E2A-HLF	primary	na	leukemia negative
B-R-25	r	BCP-ALL	E2A-HLF	primary	na	leukemia negative
T-MR-01	d	T-ALL	na	tertiary	MR	leukemia positive
T-MR-01	d	T-ALL	na	tertiary	MR	leukemia positive

*CNS engraftment was determined by HE staining of brain sections. Original samples were obtained at diagnosis (d) or at relapse (r). Risk stratification according to ALL-BFM 2000 is indicated as follows: very high risk (VHR), high risk (HR), medium risk (MR) and standard risk (SR). *represents ALL lacking the established cytogenetic abnormalities (for BCP-ALL: E2A-PBX1, E2A-HLF, BCR-ABL1, KMT2A-rearrangement, ETV6-RUNX1, high hyperdiploid or hypodiploid; T-ALL: SIL-TAL)*

Supplementary Figures

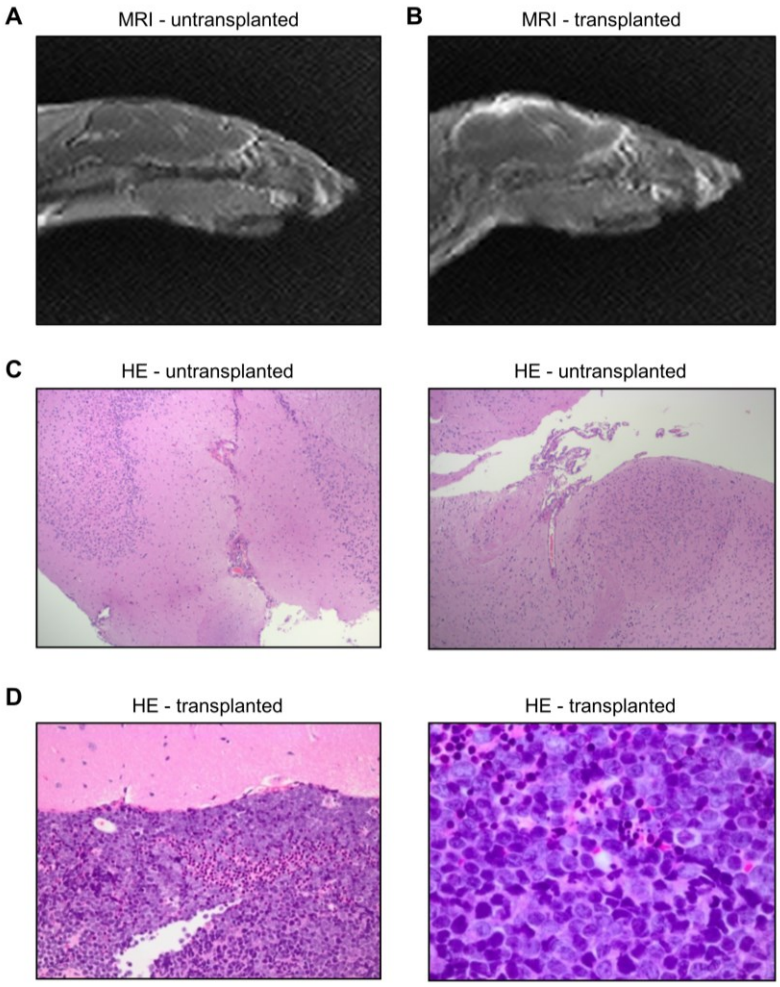

Figure S1. BCP-ALL xenografts infiltrated in the subarachnoid space of mice. (A - B) *In vivo* magnetic resonance imaging (MRI) of (A) untransplanted and (B) transplanted mice showing meningeal enhancement. Data are representative of two mice. (C - D) Histochemistry of brain section of (C) untransplanted and (D) transplanted mice. Hematoxylin-eosin staining according to standard protocols.

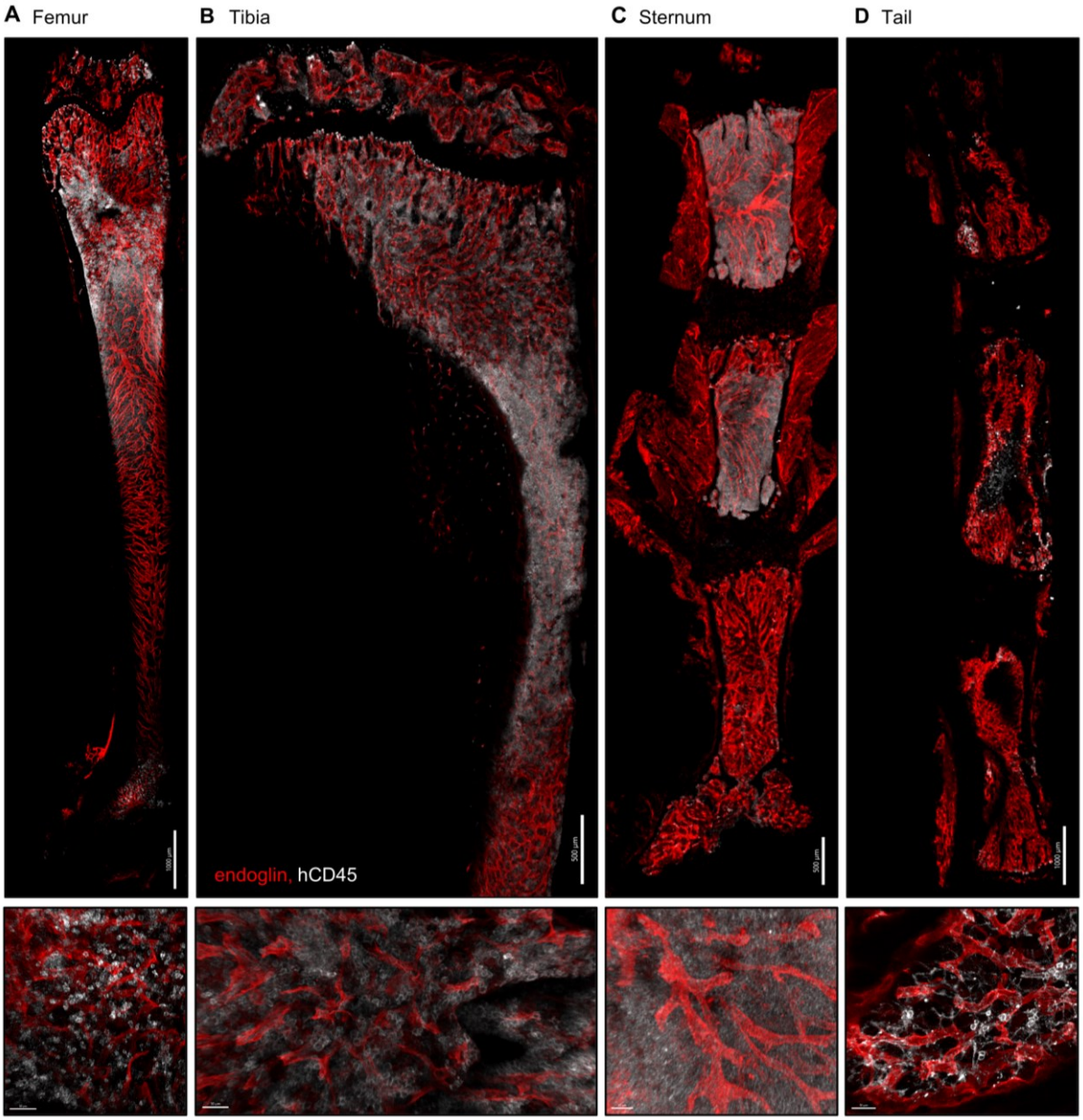

Figure S2. Leukemic engraftment in the mouse bone marrow. Images are shown of ALL cell (hCD45+, white) interactions with sinusoids (endoglin^{+}, red) for a femur (A), tibia (B), sternum (C) and tail (D) of a BCP-ALL sample taken at initial diagnosis after 6 weeks of first engraftment. Below a corresponding zoomed-in image is shown for each studied bone. Representative maximum projection of a tiled 100-300 µm z-stack confocal image. Scale bars: 50 µm on zoomed images.

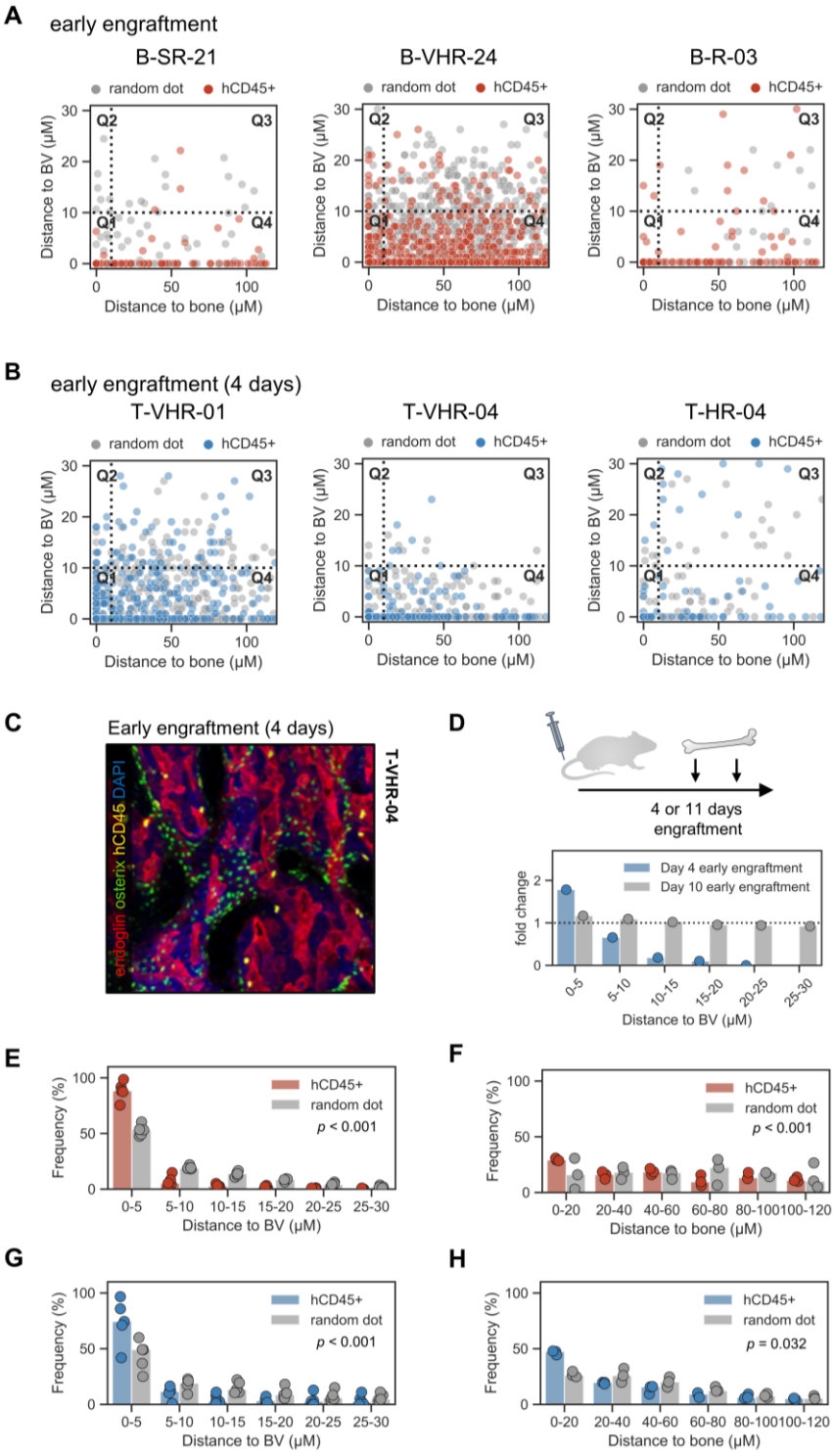

Figure S3. At early engraftment BCP- and T-ALL cells are localized in the vascular niche of bone marrow sinusoids. Distribution of mean distances of BCP-ALL (A) or T-ALL (B) cells to the bone and the bone marrow sinusoids (blood vessels, BV) at early engraftment of individual patients. (C) Distribution of T-ALL cells at early engraftment. Representative image of T-HR-04 (CD45$^+$, yellow) in spatial relationship to sinusoids (endoglin$^+$, red) and endosteum (identified by osterix$^+$, green, and DAPI$^-$, blue, signal). (D) Quantitative distance analysis of T-ALL cells to bone marrow sinusoids at different times of engraftment for T-VHR-04 compared to random dots distributed within the bone marrow tissue but outside blood vessels by using a second, independent MATLAB-based approach. Each time point represents data obtained from one bone from one individual mouse. (E, G) Binned distances of BCP-ALL (B-R-03, B-SR-21, B-SR-22, B-VHR-20 and B-VHR-24) and T-ALL (T-MR-09, T-HR-04, T-VHR-01, T-VHR-04 and T-VHR-09) cells and corresponding RD to BV. (F, H) Binned distances of BCP-ALL and T-ALL cells and corresponding RD to bone. Displayed p-values were calculated to assess the distribution differences by two-tailed Kolmogorov-Smirnov test.

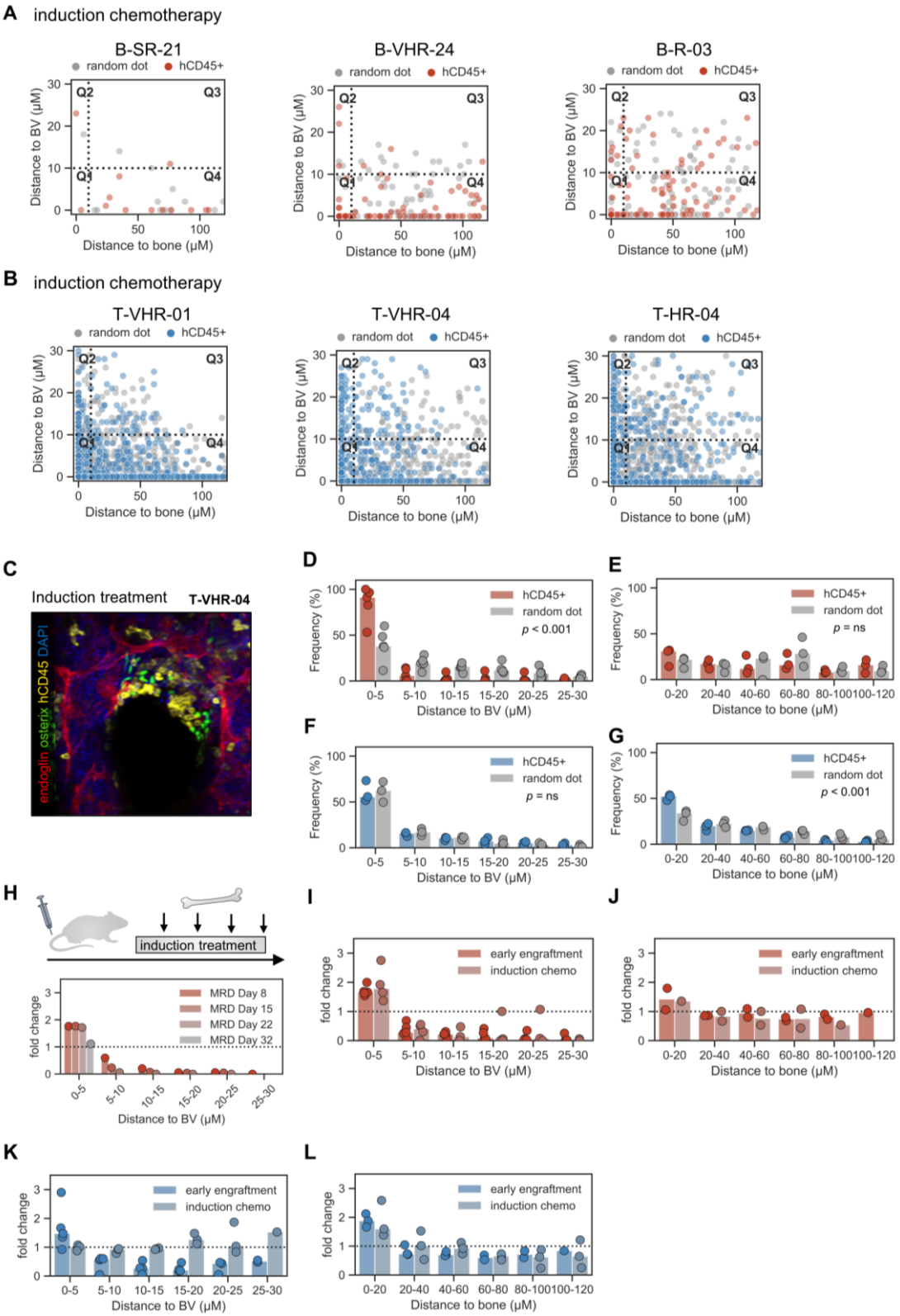

Figure S4. Upon chemotherapy T-ALL cells move towards the bone and endosteum and BCP-ALL cells localize in the perisinusoidal space. Distribution of mean distances of BCP-ALL (A) or T-ALL (B) cells to the bone and the bone marrow sinusoids (blood vessels, BV) after induction chemotherapy of individual patients. (C) Distribution of T-ALL cells after induction therapy regimen. Representative image of T-HR-04 (CD45^{+}, yellow) in spatial relationship to sinusoids (endoglin^{+}, red) and endosteum (identified by osterix^{+}, green, and DAPI^{-}, blue, signal). (D,F) Binned distances of BCP-ALL and T-ALL cells and corresponding RD to BV. (E,G) Binned distances of BCP-ALL and T-ALL cells and corresponding RD to bone. Quantitative distance analysis followed by binwise normalization of leukemic cells over computed random dots to bone marrow sinusoids and/or bone successive during chemotherapy treatment for B-VHR-20 (H) or after induction treatment of BCP-ALL (I, J) or T-ALL (K, L) PDXs were presented. Bins containing less than 10 RDs were omitted. For the MRD time points each graph represents data obtained from one bone from one mouse. For assessment after induction treatment data was pooled from n = 3 animals transplanted with the individual patient material. Displayed p-values were calculated to assess the distribution differences by two-tailed Kolmogorov-Smirnov test.

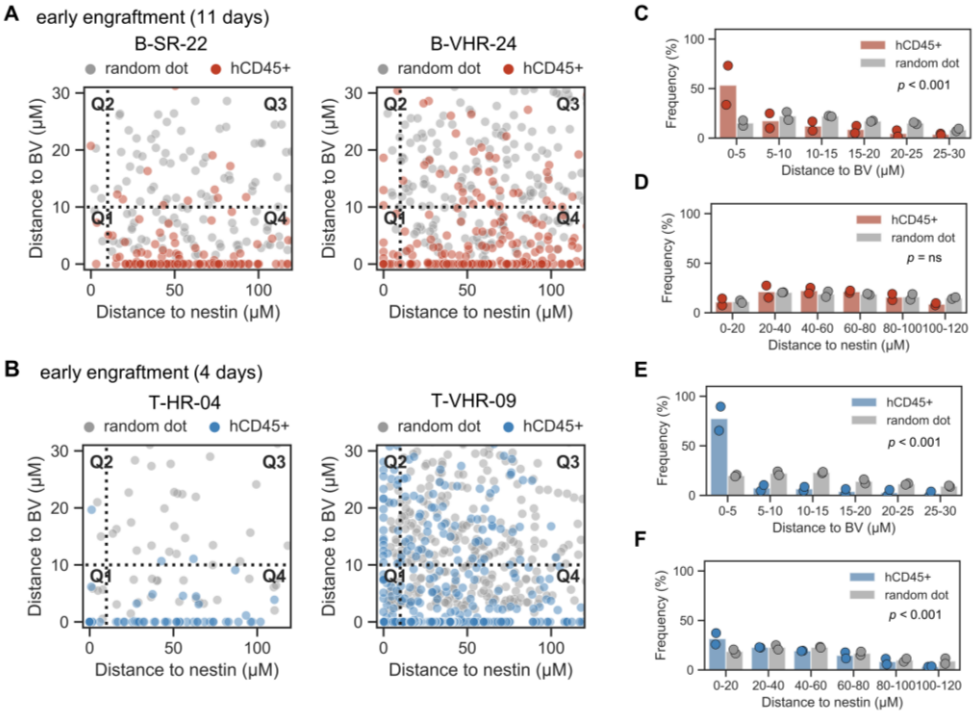

Figure S5. T-ALL cells engraft in close proximity to nestin⁺ cells. Distribution of mean distances of BCP-ALL (A) or T-ALL (B) cells to nestin⁺ cells and the bone marrow sinusoids (blood vessels, BV) at early engraftment of individual patients. (C, E) Binned distances of BCP-ALL and T-ALL cells and corresponding RD to BV. (D, F) Binned distances of BCP-ALL and T-ALL cells and corresponding RD to nestin⁺ cells. Displayed p-values were calculated to assess the distribution differences by two-tailed Kolmogorov-Smirnov test.

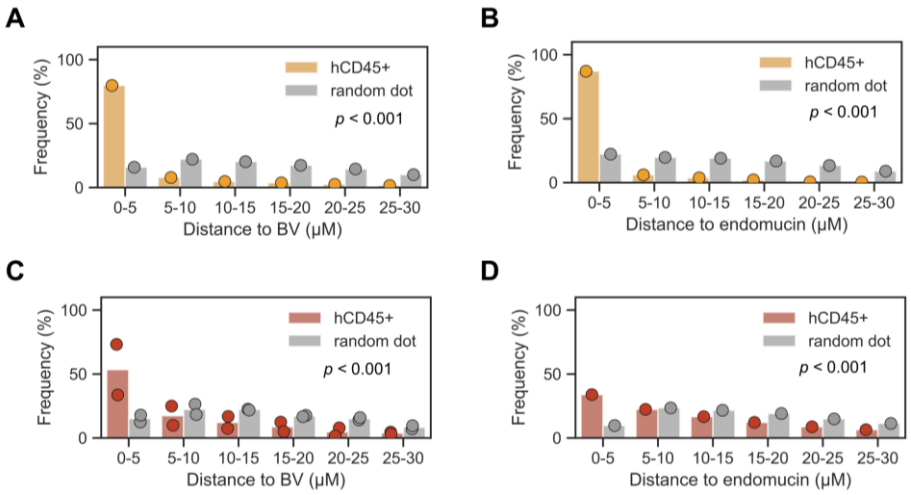

Figure S6. ALL cells and HSPCs are in proximity with bone marrow sinusoids but ALL cells not with endomucin^{high}endoglin^{low} cells. (D,G) Binned distances of HSPC (D) or BCP-ALL cells (G) and corresponding RD to BV. (E,H) Binned distances of HSPC (E) or BCP-ALL cells (H) and corresponding RD to endomucin. Displayed p-values were calculated to assess the distribution differences by two-tailed Kolmogorov-Smirnov test.

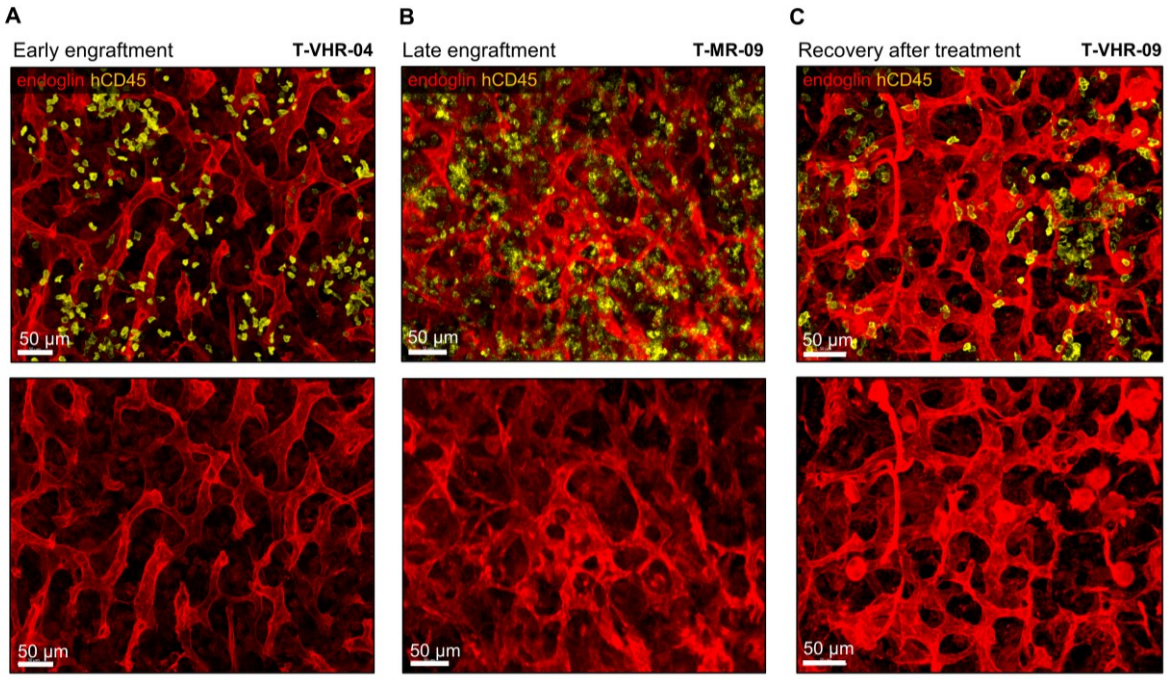

Figure S7. Vascular changes in bone marrow sinusoids upon chemotherapy T-ALL cells. Effects of early engraftment (A), vascular remodeling at late engraftment (B) and recovery after induction treatment (C) of T-ALL cells (hCD45^{+}, yellow) on the structure of bone marrow sinusoids (endoglin^{+}, red). Confocal images are represented by maximal projection of tiled 100-300 µm z-stack.

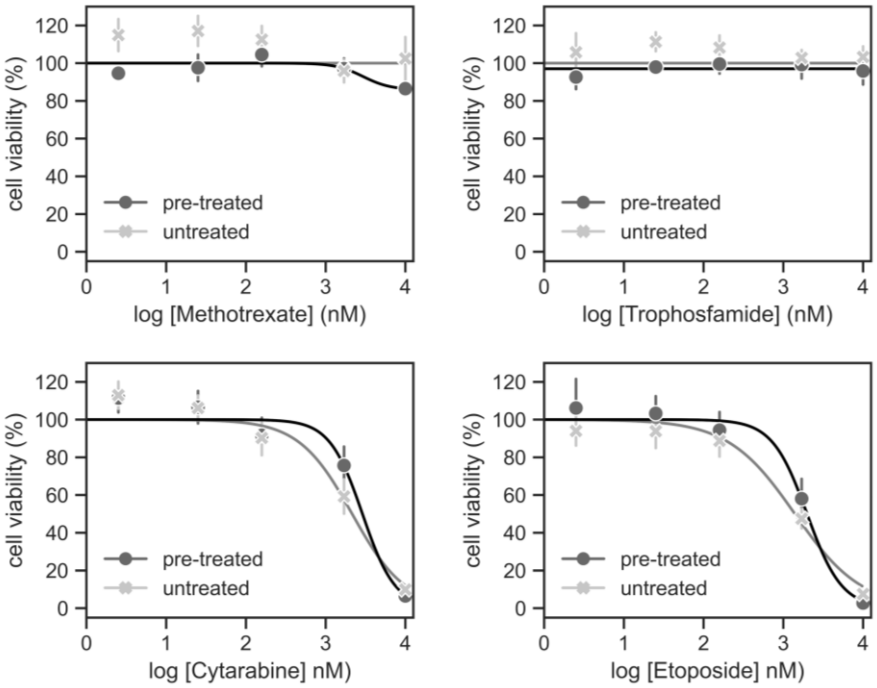

Figure S8. Chemo-selected and untreated leukemic cells do not differently respond to chemotherapeutic drugs *ex vivo*. Response of untreated ALL cells versus pre-treated ALL cells that were selected by *in vivo* combination chemotherapy to *ex vivo* treatment with etoposide, cytarabine, methotrexate or trophosfamide at indicated concentrations (n = 3 technical replicates, B-VHR-20).

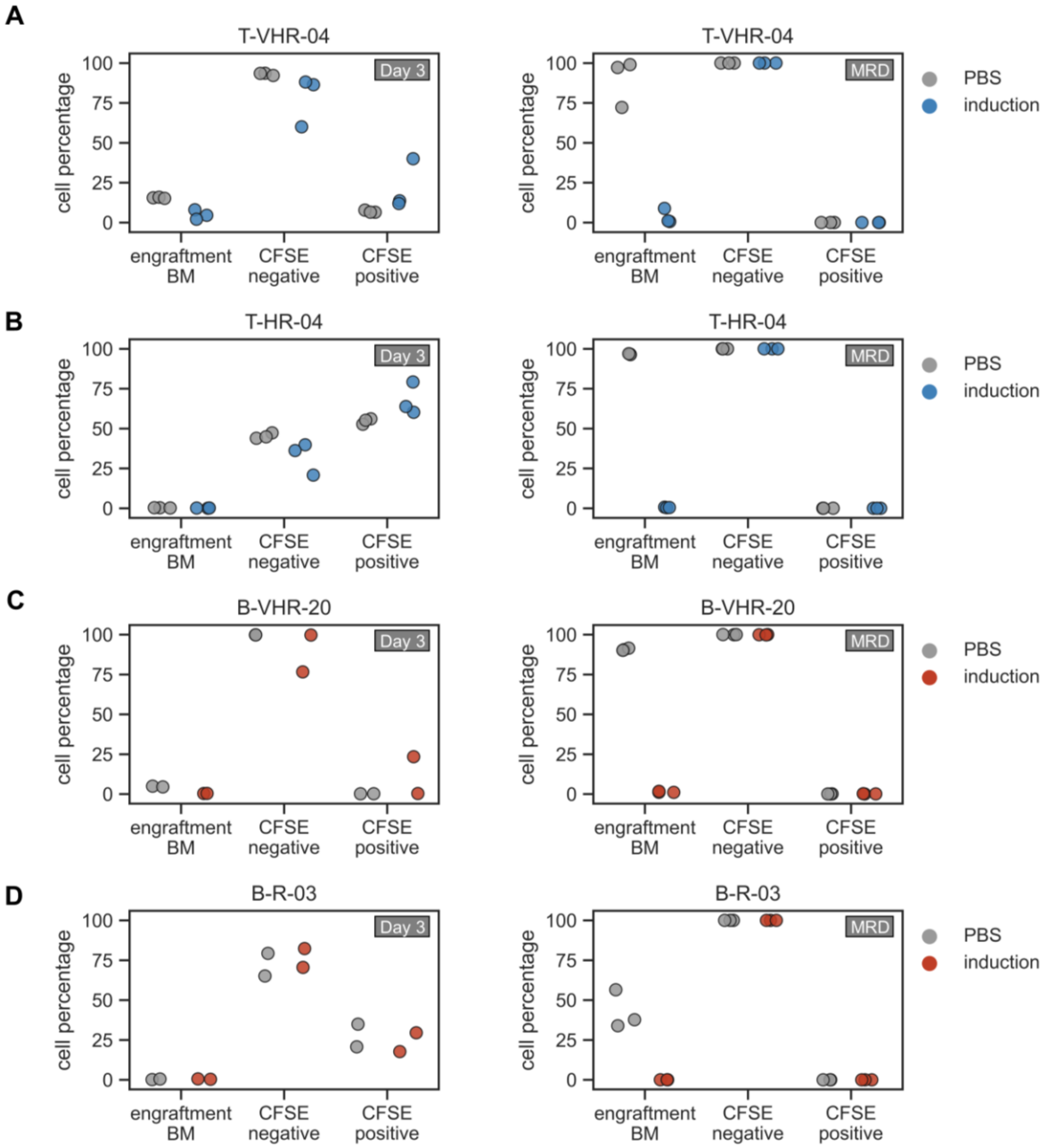

Figure S9. Upon chemotherapy leukemic cells show transiently reduced proliferative potential, without being completely dormant. (A, B, C, D) Quantification of total leukemic burden in the bone marrow of femurs and analysis of proportions of CFSE positive cells and CFSE negative cells in hCD45^{+} cell population in the bone marrow either under 3 days of chemotherapy or complete induction treatment (n = 2/3 for each patient).